744–755 Nucleic Acids Research, 1998, Vol. 26, No. 3

Solution structure of the novel antitumor drug UCH9 complexed with d(TTGGCCAA)$_2$ as determined by NMR

Ritsuko Katahira, Masato Katahira[1], Yoshinori Yamashita, Harumi Ogawa, Yoshimasa Kyogoku[2] and Mayumi Yoshida*

Tokyo Research Laboratories, Kyowa Hakko Kogyo Co. Ltd, 3-6-6 Asahimachi, Machida-shi, Tokyo 194, Japan, [1]Department of Bioengineering, Faculty of Engineering, Yokohama National University, 79-5 Tokiwadai, Hodogaya-ku, Yokohama 240, Japan and [2]Institute for Protein Research, Osaka University, 3-2 Yamadaoka, Suita, Osaka 565, Japan

Received October 24, 1997; Revised and Accepted December 2, 1997

ABSTRACT

Aureolic acid group compounds, such as chromomycin A$_3$ (CHM) and mithramycin (MIT), are known as antitumor drugs. Recently we isolated a novel aureolic acid group antitumor drug, UCH9, from *Streptomyces* sp. The chemical structure of UCH9 is unique in that mono- (A ring) and tetrasaccharide (B–E rings) segments and a longer hydrophobic sidechain are attached to the chromophore, while di- and trisaccharide segments and a methyl group are attached to it in the cases of CHM and MIT. It has been shown by two-dimensional agarose gel electrophoresis that the three drugs cause DNA unwinding, UCH9 causing less than the others. A photo-CIDNP experiment has revealed that UCH9 binds to the minor groove of DNA. The structure of the UCH9–d(TTGGCCAA)$_2$ complex has been determined by ^{1}H NMR and simulated annealing calculations. The obtained structure indicates that UCH9 binds as a dimer to the minor groove of d(TTGGCCAA)$_2$, like CHM and MIT, but that the structural change in DNA induced on binding of UCH9 is moderate in comparison with those on binding of the other two drugs. It turns out that the dimer structure of UCH9, stabilized presumably through a hydrophobic interaction involving the A, D and E rings and the hydrophobic sidechain is different from that of CHM and thus DNA can interact with UCH9 in the minor groove with a moderate structural change.

INTRODUCTION

Antitumor drugs such as chromomycin A$_3$ (CHM) and mithramycin (MIT) (Fig. 1A and B respectively), which were isolated from *Streptomyces* sp., have been extensively studied *in vivo* and *in vitro* (1,2). They are composed of a chromophore, a hydrophilic sidechain, a disaccharide segment (A and B rings) and a trisaccharide segment (C, D and E rings) (Fig. 1A and B). They form a Mg^{2+}-coordinated dimer in solution (3–8). They bind to a G/C-rich region of DNA in the presence of Mg^{2+} (9) and terminate RNA synthesis (10,11). It was shown that MIT suppresses binding of transcription factor Sp1 to a c-*myc* promoter region (12). NMR studies on CHM–DNA complexes revealed that CHM binds to a GpC site as a Mg^{2+}-coordinated dimer in the minor groove of DNA (13–15). On binding of CHM the DNA structure changes from the B-form to the A-form to accommodate the bulky CHM dimer (13–15). A similar but smaller structural change was also reported for MIT–DNA complexes (16–19).

Recently we isolated a novel aureolic antitumor drug, UCH9 (Fig. 1C), from *Streptomyces* sp. (20,21). UCH9 is composed of a chromophore, a hydrophilic sidechain, a hydrophobic sidechain, a monosaccharide segment (A ring) and a tetrasaccharide segment (B–E rings). The chemical structure of UCH9 is different from those of CHM/MIT; (i) CHM/MIT possess di- and trisaccharide segments, while UCH9 possesses mono- and tetrasaccharide segments; (ii) a methyl group is attached to C7 of the chromophores of CHM/MIT, while a longer hydrophobic sidechain, a secondary butyl group, is attached at this position of UCH9. Fast atom bombardment mass spectroscopy (FABMS) and atomic absorption analysis revealed that UCH9 isolated from *Streptomyces* sp. is a dimer containing one equimolar Mg^{2+} ion (21).

It would be interesting to study the interaction of UCH9 with DNA and to compare the interaction with those of CHM and MIT. It was suggested that MIT unwinds DNA (22). Thus the ability of DNA unwinding has been compared among the three drugs CHM, MIT and UCH9 by means of two-dimensional agarose gel electrophoresis. Then the photo-CIDNP method was used to examine whether UCH9 binds to DNA in the minor or major groove. This method was applied to a CHM–DNA complex and binding of CHM in the minor groove was revealed (23). Finally, the three-dimensional structure of a UCH9–d(TTGGCCAA)$_2$ complex has been determined by ^{1}H NMR and simulated annealing calculations. The obtained structure has been compared with that of CHM–d(AAGGCCTT)$_2$, for which atomic coordinates are available (15).

MATERIALS AND METHODS

Oligonucleotide preparation

A self-complementary octanucleotide, d(TTGGCCAA), was synthesized on the 10 µmol scale using an automated version of the phosphoramidite coupling method with a model 381A DNA synthesizer (Applied Biosystems). The octanucleotide was

*To whom correspondence should be addressed. Tel: +81 427 25 2555; Fax: +81 427 26 8330; Email: myoshida@kyowa.co.jp

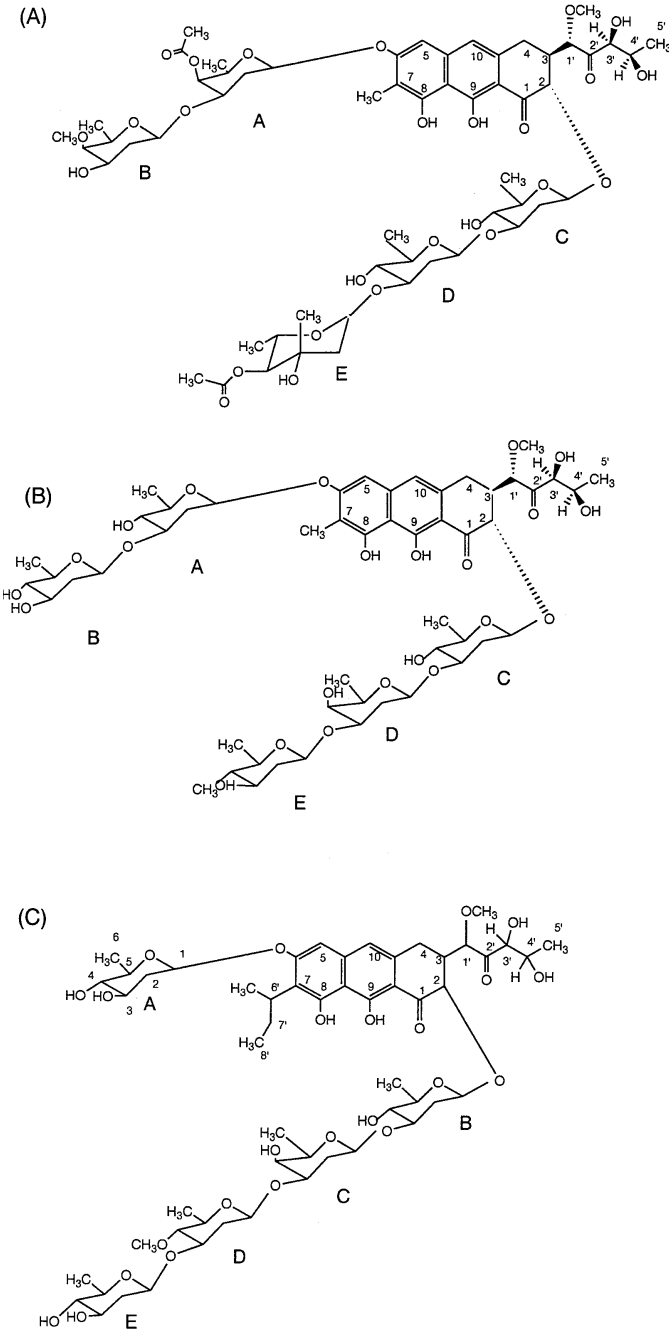

Figure 1. Chemical structures of chromomycin A_3 (CHM) (**A**), mithramycin (MIT) (**B**) and UCH9 (**C**).

purified by reverse phase HPLC, followed by Sephadex G-10 gel filtration. Finally, the counter cations were replaced first with pyridinium ions and then with sodium ions using Dowex 50 cation exchange columns (24,25).

Determination of the binding constant of UCH9 as to calf thymus DNA

The binding constant of UCH9 to calf thymus DNA was determined from a Scatchard plot (26) of the changes in UV absorption of UCH9 during titration of calf thymus DNA. The absorption spectra were recorded with a Hitachi U-200 spectrophotometer. The absorbance of UCH9 at 450 nm in the course of titration of calf thymus DNA was analyzed by the following equation

$$r/C_f = K_0(n - r), \quad \mathbf{1}$$

where $r = C_b/C_p$, C_b and C_f are the concentrations of bound and free UCH9 respectively, C_p is the concentration of calf thymus DNA, n is the number of binding sites per nucleotide and K_0 is an intrinsic binding constant. The concentration of bound ligand was estimated by the following equation

$$C_b = \Delta A/(\varepsilon_b - \varepsilon_f), \quad \mathbf{2}$$

where ΔA is the increase in absorbance on addition of calf thymus DNA and ε_b and ε_f are the molar extinction coefficients of bound and free UCH9 respectively.

DNA unwinding assay

Bacteriophage T4 DNA ligase, restriction endonuclease *Hin*dIII and plasmid pBR322 were purchased from Takara Shuzo Co. pBR322 DNA was linearized with *Hin*dIII and recovered by phenol extraction and ethanol precipitation. Each drug, CHM, UCH9 and MIT, was dissolved in dimethyl sulfoxide at 1 mM and diluted in methanol containing 40% dimethyl sulfoxide before use. The solvent used for diluting the drugs (5% of the total volume of the reaction mixture) did not affect enzyme activity. The reaction mixture (200 µl), comprising 66 mM Tris–HCl, pH 7.6, 6 mM $MgCl_2$, 10 mM dithiothreitol, 0.7 mM ATP, 0.6 µg linearized DNA and each drug, was equilibrated at 15°C for 10 min. Then the reaction mixture was incubated with an excess amount of T4 DNA ligase at 15°C (controlled within ±0.5°C) for 60 min. The drug was then extracted with phenol and ether. DNA was precipitated with ethanol to remove the remaining drug and then analyzed by two-dimensional agarose gel electrophoresis (27). After the first electrophoresis the gel was rotated by 90° and then the second electrophoresis was carried out with 0.5 µg/ml ethidium bromide.

NMR spectroscopy

One-dimensional normal and photo-CIDNP difference spectra were recorded with a Bruker ARX 500 spectrometer at 30°C as described previously (23). The lyophilized octanucleotide was dissolved in 0.5 ml D_2O containing 10 mM Na phosphate buffer, pH 6.9, and 100 mM NaCl at a strand concentration of 1.0 mM. An equimolar concentration of UCH9 (1.0 mM) was added. 3-(Carboxymethyl)lumiflavin (flavin I) was synthesized from lumiflavin purchased from Sigma Co. (28) and added to the DNA solution (0.2 mM). DSS was used as an internal reference. Laser power for irradiation was 0.8 W and the irradiation time was 300 ms. The repetition delay was 5 s and 32 free induction decays were accumulated. No significant flavin bleaching was detected visually under the present experimental conditions.

Other NMR spectra were recorded with Bruker AM 500 and DMX 500 spectrometers. The lyophilized octanucleotide was dissolved in 0.25 ml D_2O or H_2O containing 10 mM Na phosphate buffer, pH 6.9, and 100 mM NaCl at a strand concentration of 2 mM. Mg^{2+}-coordinated UCH9 was added gradually, the final concentration of UCH9 being 2 mM. A NOESY spectrum (29), with a mixing time of 150 ms, was recorded in H_2O at 15°C using a water flip-back sequence (30) as detection pulse. DQF-COSY

(31), E.COSY (32) and NOESY spectra with mixing times of 80 and 200 ms were recorded in D_2O at 30°C. The time domain data sets consisted of 1024 complex data for t_2 and 512 increments for t_1. The repetition delay was 2.0 s. All data were processed with Xwinnmr (Bruker) and TRIAD NMR (Tripos Inc.) software. The free induction decays were apodized with a sine-square function shifted by $\pi/3$ in both the t_1 and t_2 dimensions. Spectral resolution was enhanced by zero filling to 4096 points in the t_2 dimension (1.05 Hz/point) and 2048 points in the t_1 dimension for the DQF-COSY and E.COSY spectra. Baseline correction with a polynomial function was performed for each dimension.

Structure determination

The structure calculation was carried out with X-PLOR (33) on an Indigo R8000 computer. The parameters parallhdg.dna and quanta.xpl were used for DNA and UCH9 respectively. The intensities of cross-peaks in the NOESY spectrum with a mixing time of 80 ms were classified into three categories, strong, medium and weak. Distance restraints of 2.0–3.0, 2.0–4.0 and 2.0–6.0 were applied for each category. In total 416 distance restraints (68 distance restraints for intramolecular interactions within a UCH9 monomer, 66 distance restraints for intermolecular interactions between UCH9 monomers, 70 distance restraints for intraresidue interactions of DNA, 90 distance restraints for inter-residue interactions of DNA, 90 distance restraints for intermolecular interactions between UCH9 and DNA and 32 hydrogen bond restraints of base pairs of DNA) were incorporated in the calculation with a force constant of 50 kcal/mol/^{2}. The H1′–H2′ and H1′–H2″ coupling constants of DNA were obtained from the E.COSY spectrum. On the basis of these coupling constants 16 dihedral angle restraints for δ, C5′-C4′-C3′-O3′, of DNA sugars were incorporated with a force constant of 200 kcal/mol/rad^2. Qualitative analyses of NOESY and E.COSY spectra indicated that all of the rings of UCH9 take on the chair form. Therefore, 36 dihedral angle restraints were applied to keep the rings in the chair form for H1-C1-C2-H2a, H2a-C2-C3-H3, H3-C3-C4-H4 and H4-C4-C5-H5 of the A, B, D and E rings and for H1-C1-C2-H2a and H2a-C2-C3-H3 of the C ring. Planarity restraints were incorporated to keep DNA base pairs flat (33). Additionally, the backbone dihedral angles of DNA were restrained weakly as follows to keep a right-handed helical structure: α, –70 ± 50°; β, 180 ± 50°; ε, 180 ± 50°; ζ, –85 ± 50°. These restraints are weak enough to cover both canonical A-form and B-form structures (34).

The coordination of Mg^{2+} with a CHM dimer was reported and Mg^{2+} coordinated to O1 and O9 of the two CHM monomers (15). The ^{13}C NMR chemical shifts of C1 and C9 of UCH9 suggested the same coordination for UCH9 (21). Thus we applied the restraints to keep the same Mg^{2+} coordination in the UCH9 dimer as in the CHM dimer. The Mg^{2+}–O1 and Mg^{2+}–O9 distances were restrained to 2.64 . The O1–Mg^{2+}–O9 and O9–Mg^{2+}–O9* (* denotes another monomer) angles were restrained to 180 and 90° respectively, with a force constant of 10 kcal/mol/rad^2.

Canonical A- and B-forms (34) were used as initial DNA structures. An initial UCH9 dimer structure was produced on the basis of the coordinates of the CHM dimer (15). DNA and UCH9 were initially located 10 Å apart in order to determine the arrangement of the two molecules purely from the intermolecular NOEs between them. In order to maintain a two-fold symmetry, the NCS (non-crystallographic symmetry) function (33) was incorporated during the calculation. High temperature dynamics at 1000 K were carried out for 30 ps, which was followed by a cooling step to 100 K for 15 ps with a standard X-PLOR protocol, sa.inp. The structure was refined further with another standard X-PLOR protocol, refine.inp. In the sa.inp and refine.inp protocols an electrostatic energy term is not included. The structures were drawn with the use of QUANTA (MSI). Helical parameters were calculated by the use of NEWHEL93.

RESULTS

The binding constant of Mg^{2+} to UCH9 and the binding constant of Mg^{2+}-coordinated UCH9 to calf thymus DNA

Both CHM and MIT form two different kinds of Mg^{2+}–drug complexes, complexes I and II (4–8). In complex I one Mg^{2+} binds to a drug monomer, while in complex II one Mg^{2+} binds to a drug dimer. Complex I and complex II can be distinguished by their characteristic UV spectra. The UV spectrum of UCH9 was the same as that of complex II (data not shown). This is consistent with the finding on FABMS and atomic absorption analysis that UCH9 isolated from *Streptomyces* sp. is a dimer containing one equimolar Mg^{2+} ion (21). The binding constants of Mg^{2+} to the CHM dimer and the MIT dimer are both of the order of 1×10^3/M. The UV spectrum of UCH9 was obtained at a UCH9 concentration of 10 µM without explicit addition of Mg^{2+} to the solution. This indicates that the binding constant of Mg^{2+} to the UCH9 dimer is significantly higher than those to the CHM and MIT dimers.

From a Scatchard plot the binding constant of Mg^{2+}-coordinated UCH9 to calf thymus DNA was determined to be 1.2×10^5/M with *n*, the number of binding sites per nucleotide, being 0.1 (data not shown). The binding constant of Mg^{2+}-coordinated CHM to calf thymus DNA was 1.0×10^5/M, with *n* being 0.18, and that of Mg^{2+}-coordinated MIT to calf thymus DNA was 1.1×10^5/M, with *n* being 0.21 (6,7). Thus the binding constant of Mg^{2+}-coordinated UCH9 to DNA was of the same order as those of Mg^{2+}-coordinated CHM and MIT to DNA.

Comparison of DNA unwinding caused by CHM, UCH9 and MIT

MIT was suggested to unwind DNA on the basis of the results of qualitative one-dimensional electrophoresis (22). We analyzed DNA unwinding caused by CHM, UCH9 and MIT quantitatively by means of two-dimensional agarose gel electrophoresis (Fig. 2). CHM produced negatively supercoiled bands at 0.5 µM. By comparing the most populated bands obtained with and without the drug the linking number difference (ΔL_k) between with 0.5 µM CHM and with no drug [(+) in Fig. 2] was determined to be ~–8 to –9. Similarly, MIT shifted the equilibrium toward negative supercoiling and ΔL_k was ~–2 at 0.5 µM MIT, which indicates that DNA unwinding by MIT was less than that by CHM. No significant difference in linking number was detected at 0.5 µM UCH9 (ΔL_k was almost 0). Even at the highest UCH9 concentration (50 µM) the pattern of bands was similar to that at 0.5 µM MIT. The binding constant of UCH9 to DNA was almost the same as those of CHM and MIT and *n* for UCH9 was smaller than those for CHM and MIT by a factor of only 2. Thus it was concluded that DNA unwinding caused by UCH9 is very moderate in comparison with that by CHM and MIT.

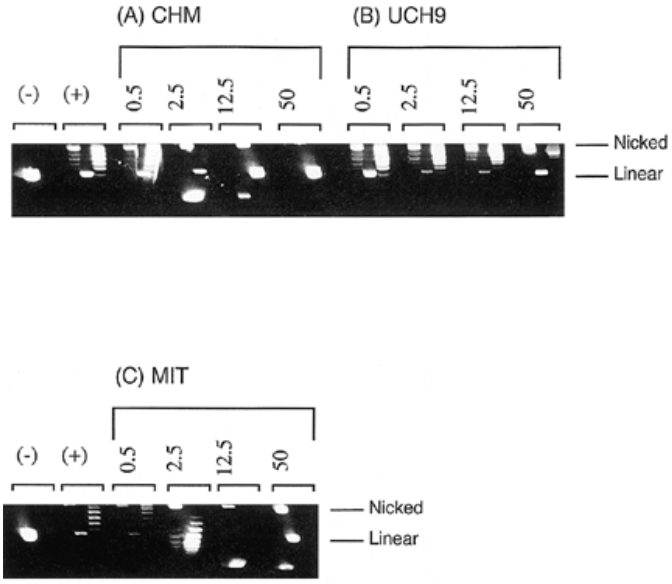

Figure 2. Two-dimensional agarose gel electrophoresis to reveal the DNA unwinding caused by various concentrations (0.5, 2.5, 12.5 and 50 µM) of each drug: CHM (**A**), UCH9 (**B**) and MIT (**C**). After extraction of each drug the ligated DNA was electrophorated from top to bottom. The gel was soaked in a 0.5 µg/ml ethidium bromide solution and then the second electrophoresis was carried out in the presence of ethidium bromide from left to right. (+) denotes the lane for the DNA ligated in the absence of any drug and (–) the lane for the substrate linear DNA. The positions of nicked and linear DNA are indicated on the right as Nicked and Linear respectively.

Stoichiometry of the complex between UCH9 and d(TTGGCCAA)$_2$

The stoichiometry of the complex was determined on the basis of the intensity changes in ^{1}H NMR signals with gradual addition of a Mg^{2+}-coordinated UCH9 dimer to d(TTGGCCAA)$_2$. When UCH9 was added the intensities of the resonances originating from free d(TTGGCCAA)$_2$ decreased, while those of new ones originating from the complex increased (data not shown). When the ratio of UCH9 dimer to d(TTGGCCAA)$_2$ reached 1:1 the resonances of free d(TTGGCCAA)$_2$ disappeared completely. During addition of UCH9 no heterogeneous resonance resulting from breakage of the two-fold symmetry was observed. These results indicate that the complex consists of a UCH9 dimer and a d(TTGGCCAA)$_2$ duplex at all times during addition of UCH9.

Suppression of the CIDNP signal of d(TTGGCCAA)$_2$ on complex formation

The photo-CIDNP technique has been applied to proteins to study their surfaces and their interactions with ligands (35). We applied this technique to structural studies on nucleic acids (23). A CIDNP signal was observed for A-form and B-form nucleic acids, but not for Z-form ones. Taking into account the structural feature that the minor groove of the Z-form is narrow and deep in comparison with those of the A- and B-forms (38), it is suggested that access of a flavin molecule to a base in the minor groove and the resulting photoreaction are required for appearance of the CIDNP signal.

The lower part of Figure 3A is the photo-CIDNP difference spectrum of d(TTGGCCAA)$_2$ in the absence of UCH9. The

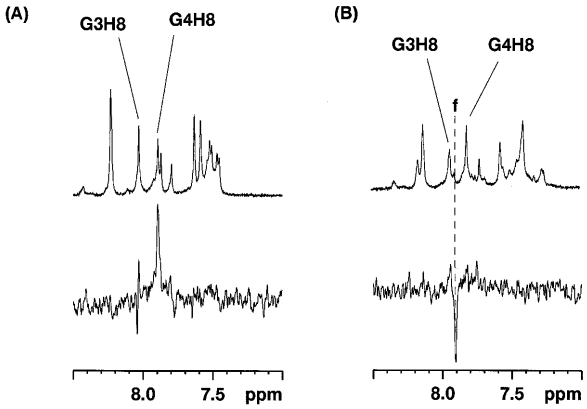

Figure 3. One-dimensional normal (upper) and photo-CIDNP difference (lower) spectra of d(TTGGCCAA)$_2$ (**A**) and the d(TTGGCCAA)$_2$–UCH9 complex (**B**) in 10 mM phosphate buffer containing 0.1 M NaCl, pH 6.9, at 30°C. f indicates flavin I.

assignments were made as mentioned later. H8 of the central residue, G4, gave a strong CIDNP signal. It is interesting that a CIDNP signal was observed for the central G4 residue exclusively but not for the neighboring G3 residue. This might be due to the difference between the two residues in affinity for a flavin molecule. On addition of UCH9 the CIDNP signal was suppressed (the lower part of Fig. 3B). Prior to this experiment the effect of addition of UCH9 on the CIDNP signal of 5′-GMP, which does not interact with UCH9, was examined. The intensity of the CIDNP signal observed for H8 of 5′-GMP was unaffected by addition of UCH9 (data not shown). Therefore, suppression of the CIDNP signal of G4H8 on addition of UCH9 is thought to indicate that UCH9 interferes with access of a flavin molecule to the G4 base in the minor groove by sitting in the minor groove at around G4. Similar suppression of the CIDNP signal was observed on binding of CHM to the minor groove of d(GGGGCCCC)$_2$ (23).

Assignments of proton resonances of drug-free d(TTGGCCAA)$_2$ and DNA-free UCH9 respectively

The octanucleotide sequence used in this study was the same as that used in a study on the CHM–d(TTGGCCAA)$_2$ complex, thus the assignments of drug-free d(TTGGCCAA)$_2$ were available (13). However, the concentration of DNA used in the previous study (strand concentration 3.1 mM) was higher than that used in this study (strand concentration 2 mM) and the experimental conditions were slightly different. Thus we reassigned the resonances of the DNA. The assignments were completed in the same manner as for other DNAs (21) and were consistent with those reported in the literature.

Assignments of proton resonances of a Mg^{2+}-coordinated UCH9 dimer have already been completed in $CDCl_3/CD_3OD$ solution and reported (21). Because of aggregation, assignments for UCH9 in aqueous solution were not carried out.

Assignments of proton resonances in the complex

Exchangeable protons. The exchangeable protons of d(TTGGCCAA)$_2$ and UCH9 in the complex were assigned by use of a NOESY spectrum in 90% H_2O/10% D_2O at 15°C (Fig. 4A). The imino proton of T2 was identified from the NOE

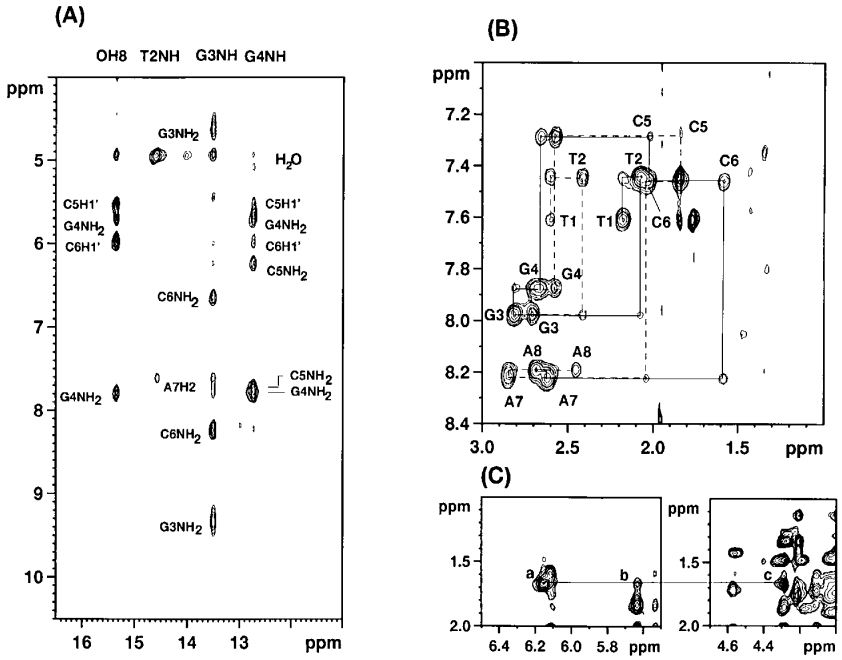

Figure 4. (**A**) Expansion of the NOESY spectrum of the UCH9–d(TTGGCCAA)$_2$ complex in 90% H_2O/10% D_2O containing 10 mM phosphate buffer and 0.1 M NaCl, pH 6.9, at 15°C, indicating NOEs involving OH8 and imino protons. (**B**) Expansion of the H6/H8–H2′/H2″ region of the NOESY spectrum of d(TTGGCCAA)$_2$ in the complex at 30°C. The connectivities between H6/H8 and H2′ and those between H6/H8 and H2″ are shown by solid and broken lines respectively, intraresidue cross-peaks being labeled. (**C**) Expansion of the NOESY spectrum of the complex at 30°C indicating the intermolecular NOEs involving Me6′ of UCH9: Me6′–G4H1′ (a), Me6′–C5H1′ (b) and Me6′–G4H4′ (c) NOEs.

from A7H2. The G3 and G4 imino protons were identified from the sequential imino–imino NOEs between T2 and G3 and between G3 and G4. The amino protons of C5 and C6 were identified from the NOE from H5 of each residue and the NOE from the imino proton of base paired G4 and G3 respectively. The amino protons of G3 and G4 were identified from the NOE from the imino proton of each residue. The strong NOEs between the imino protons of G (G3 and G4) and the amino protons of C (C6 and C5) indicate the formation of Watson–Crick G:C base pairs. An additional exchangeable resonance was observed at 15.38 p.p.m. in Figure 4A. Strong NOEs were observed to this resonance from H6′, Me6′, H7′ and H8′ of UCH9 and thus this resonance was assigned as OH8 of UCH9. Assignments of the exchangeable protons of d(TTGGCCAA)$_2$ and UCH9 in the complex are listed in Table 1.

Non-exchangeable protons. Assignments of non-exchangeable protons of d(TTGGCCAA)$_2$ in the complex were completed by use of NOESY and DQF-COSY spectra in D_2O at pH 6.9 and 30°C, in the same way as reported for other DNAs (24,25). As an example of the assignment procedure Figure 4B shows the sequential H6/H8–H2′/H2″ connectivities in the NOESY spectrum. It is remarkable that the intraresidue H6–H2′ and H6–H2″ cross-peaks are very weak for C5. The intraresidue H6–H2′ cross-peak is also relatively weak for C6. These results suggest that the structure of the C5–C6 portion deviates from the B-form (36). The distinction between H2′ and H2″ was made by comparison of the intensities of the H1′–H2′ and H1′–H2″ NOESY cross-peaks. The non-exchangeable proton assignments of d(TTGGCCAA)$_2$ in the complex are listed in Table 1.

The non-exchangeable protons of UCH9 in the complex were assigned by use of the NOESY and DQF-COSY spectra in the same way as for CHM in a complex (24). The aromatic chromophore protons H5 and H10 were easily identified because they appeared apart from the other signals. The other chromophore protons were assigned from the NOEs from these aromatic protons. The hydrophobic sidechain of UCH9 was assigned on the basis of the scalar connectivities between H8′ and H7′, H7′ and H6′ and H6′ and Me6′. The hydrophilic sidechain, which is the same as that of CHM, was assigned in the same way as reported previously (24). The A ring protons were assigned from the NOEs from H5 and H10 of the chromophore. The B ring protons were assigned from the NOEs from H2 of the chromophore. The following C–E rings were assigned from the NOEs between H2 of a ring and H3 and H4 of the preceding ring. The assignments of non-exchangeable protons of UCH9 in the complex are listed in Table 1.

Changes in the chemical shifts on complex formation

The changes in chemical shifts of d(TTGGCCAA)$_2$ on complex formation were calculated (supplementary material, Table 1S). Large changes of >0.2 p.p.m. were observed for the C5–C6 segment exclusively. This suggests that the central segment, composed of C5–C6 and the complementary G3–G4 of the two strands, is the binding site of UCH9. It was remarkable that the C5H4′ resonance is shifted upfield by 2.34 p.p.m. on complex formation.

The chemical shift differences of dimeric UCH9 between the complex state in aqueous solution and the free state in CD_3OD/$CDCl_3$ solution were also calculated (supplementary material, Table 1S). Differences of >0.2 p.p.m. on complex formation were observed for H1, H2e, H3 and H5 of the A ring, H2a, H4 and H5 of the B ring, H2e, H2a and H4 of the D ring and H1, H2e, H3 and H5 of the E ring.

Table 1. ^{1}H NMR chemical shifts of d(TTGGCCAA)$_2$ and UCH9 in the complex (p.p.m.)

d(TTGGCCAA)$_2$									
Residue	H6/H8	H2/H5	H1′	H2′	H2″	H3′	H4′	NH	NH_{2b}[a]/NH_{2e}[b]
T1	7.62	1.77	6.10	2.17	2.60	4.78	4.17	n.o.[c]	–
T2	7.44	1.85	5.88	2.07	2.41	4.92	4.18	14.66	–
G3	7.97	–	5.47	2.81	2.70	5.09	4.41	13.58	9.40/4.67
G4	7.87	–	6.15	2.65	2.57	5.07	4.30	12.80	7.87/5.78
C5	7.29	5.20	5.64	2.02	1.83	4.28	1.87	–	7.80/6.32
C6	7.46	5.47	6.12	1.58	2.04	4.83	4.12	–	8.30/6.71
A7	8.23	7.78	6.12	2.60	2.84	5.02	4.22	–	n.o.
A8	8.18	7.87	6.34	2.68	2.43	4.79	4.22	–	n.o.

UCH9								
Ring	H1	H2e	H2a	H3	H4	H5	H6	OMe4
A	5.34	2.70	1.89	3.99	3.20	3.78	1.45	
B	4.57	2.04	1.71	2.24	3.07	3.20	1.43	
C	3.10	1.13	1.42	3.46	3.87	3.62	1.35	
D	5.01	2.41	1.77	4.04	3.10	3.57	1.47	3.65
E	4.90	2.52	1.73	4.02	3.04	3.58	1.49	

Chromophore (Chm)							Sidechain								
H2	H3	H4e	H4a	H5	H10	OH8	H1′	H3′	H4′	H5′	OMe1′	H6′	Me6′	H7′	H8′
4.55	3.14	2.63	2.96	6.82	6.57	15.38	4.91	4.22	4.28	1.33	3.39	3.50	1.67	1.64,1.73	0.92

[a]Base paired amino proton.
[b]Non-base paired amino proton.
[c]Not observed.

Change in the sugar conformation on complex formation

The H1′–H2′/H2″ and H3′–H2′/H2″ DQF-COSY cross-peaks of d(TTGGCCAA)$_2$ in the complex are shown in Figure 5A and B respectively. It should be noted for C5 and C6 that the H1′–H2′ cross-peak is very weak and a strong to medium H3′–H2″ cross-peak is present. These results are not expected for a canonical B-form sugar pucker, C2′-*endo*, but expected for A-form sugar puckering (37). The appearance of A-form sugar puckering for C5 and C6 is consistent with the results of the NOESY experiment (Fig. 4B). For C5 and C6 in the UCH9-free state the H1′–H2′ cross peak is strong and the H3′–H2″ cross-peak is weak (data not shown), as expected for B-form sugar puckering. Thus it is concluded that the sugar conformations of C5 and C6 changed from the B-form to the A-form on complex formation. The large chemical shift differences observed for C5 and C6 exclusively on complex formation are also consistent with this conclusion. The three bond coupling constant between H1′ and H2′ obtained from the E. COSY spectrum was 2.8–3.0 Hz for C5 and C6. The coupling constant, together with the qualitative results mentioned above, indicates that the sugar puckering of C5 and C6 is about C4′-*exo* in the complex.

For the other residues the intensities of the corresponding cross-peaks in Figure 5A and B indicate that the sugars take on B-form puckering in the complex as well as in the UCH9-free state. The smaller chemical shift differences on complex formation for these residues are consistent with this. The H1′–H2′ coupling constant for these residues is ~9 Hz, which indicates that the sugar puckering is about C2′-*endo* for them.

The possibility of a dynamic equilibrium between S- and N-type sugar puckering in the complex was examined by the method originated by Altona and colleagues (39). For the C5 and C6 residues the population of N-type sugar puckering was determined to be more than 95%. For the G3 and G4 residues the population of S-type sugar puckering was >90% and for the other residues the population of S-type sugar puckering was >95%. Therefore, it was not necessary to consider the S/N equilibrium for each residue in the complex. On the basis of these results the dihedral angle restraint of 85 ± 15° was applied for δ, C5′-C4′-C3′-O3′, of C5 and C6 of the DNA and one of 140 ± 20° for δ of the other DNA residues in calculation of the complex structure. The former restraint leaves freedom for the sugar to take any conformation without an energy penalty between C3′-*endo* and O4′-*endo*, including C4′-*exo*, in a pseudorotation cycle and the latter restraint between C1′-*exo* and C3′-*exo*, including C2′-*endo* (38). Thus these restraints are relatively moderate.

Elucidation of the chemical structure of UCH9 revealed that the A, B and E rings are β-D-olivose, the D ring is 4-methoxy-β-D-olivose and the C ring is β-D-oliose (21). In the complex state strong cross-peaks were observed in the DQF-COSY spectrum between H1 and H2a, H2a and H3, H3 and H4 and H4 and H5 for the A, B, D and E rings (data not shown). For the C ring strong cross-peaks were observed between H1 and H2a and H2a and H3. The observation of these strong cross-peaks indicates that all of the rings A–E take on the chair form and not the boat form in the complex. The strong NOE cross-peaks observed for rings A–E between H1 and H3, H1 and H5 and H3 and H5 also support the chair form. A chair form was concluded for rings A–E in the free state on the basis of the same experimental results, thus the conformation of the rings of UCH9 did not change on complex formation. For the A, B, D and E rings of UCH9 the dihedral angle restraint of 180 ± 40° was applied for H1-C1-C2-H2a, H2a-C2-C3-H3, H3-C3-C4-H4 and H4-C4-C5-H5 and the same restraint was applied for H1-C1-C2-H2a and H2a-C2-C3-H3 of the C ring in the calculation in order to maintain the chair form.

NOEs between two UCH9 monomers in the complex

UCH9 consists of several segments, a chromophore, hydrophilic and hydrophobic sidechains and rings A–E. In Table 2 the NOEs

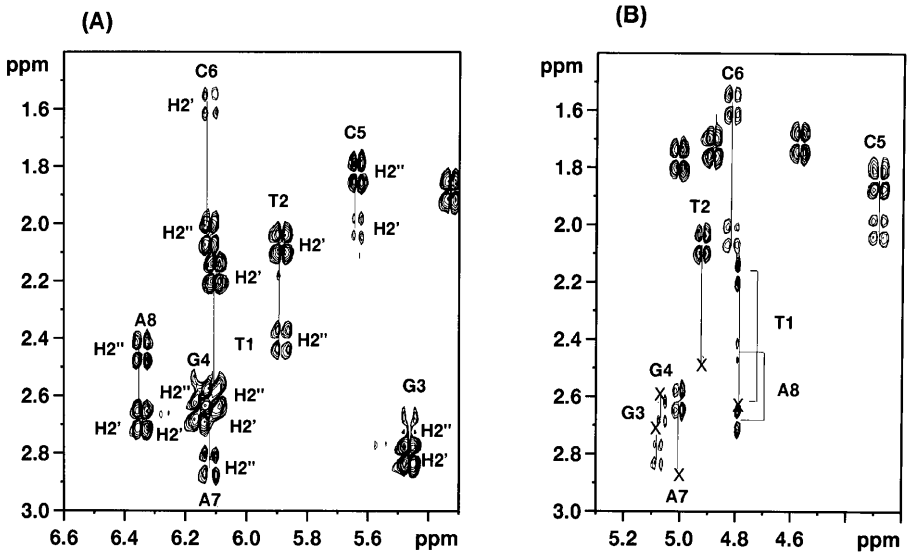

Figure 5. Expansion of the H1′–H2′/H2″ (**A**) and H3′–H2′/H2″ (**B**) regions of the DQF-COSY spectrum of d(TTGGCCAA)$_2$ in the complex at 30°C. Missing cross-peaks are denoted by X and non-labeled cross-peaks are those between H1 and H2a of the UCH9 rings.

observed between two segments of UCH9 are summarized. UCH9 forms a Mg^{2+}-coordinated dimer in solution. On the basis of simple molecular modeling, NOEs between two different UCH9 monomers are identified among the intersegment NOEs, as accomplished for the CHM dimer in a complex (24). Many NOEs were observed between C ring protons and ChmH5 and ChmH10. If these NOEs are regarded as ones within a UCH9 monomer, rings B–E should fold back to the chromophore, which would cause serious steric hindrance between the chromophore and these rings. Thus these NOEs must be ones between the two UCH9 monomers. In the same way, the following NOEs must also be intermonomer NOEs: B ring protons–ChmH4a, –ChmH5 and –ChmH10 NOEs and a DH1–ChmH5 NOE and D and E ring protons–hydrophobic sidechain H7′, –Me6′ and –H8′ NOEs. The intermonomer NOEs between saccharide segments were identified as well, A ring protons–C, –D and –E ring protons.

NOEs between UCH9 and d(TTGGCCAA)$_2$ in the complex

Assignments for UCH9 and d(TTGGCCAA)$_2$ enabled us to identify the intermolecular NOEs between them. The intermolecular NOEs are summarized in Table 3 and some of the key intermolecular NOEs are shown in Figure 4A and C. Many NOEs were detected between the hydrophobic sidechain (H6′, H7′, Me6′ and H8′) of UCH9 and DNA. In particular, strong intermolecular NOEs were observed between Me6′ and G4H1′ and G4H4′ (Fig. 4C). Many NOEs were also detected between OH8 and the G4–C6 segment (Fig. 4A). In particular, a strong NOE was observed between OH8 and G4NH$_2$. The opposite edge of the chromophore (H3, H5 and H10) also gives medium to weak intermolecular NOEs. Additionally, rings A, B, D and E give medium to weak intermolecular NOEs.

The hydrophobic sidechain must be positioned near the G3–C5 segment, as judged from the strong Me6′–G4H1′ and Me6′–G4H4′ NOEs and the many medium NOEs between the protons of the hydrophobic sidechain and the protons of the G3, G4 and C5 residues. In this situation the distances between H8′ of UCH9 and the protons of the C6 and A7 residues of the same strand are too great to observe NOEs. Thus mostly weak NOEs from H8′ to the protons of the C6 and A7 residues turned out to be NOEs to residues on the complementary strand. Similarly, the strong NOE between OH8 and G4NH$_2$ restricts the position of OH8 close to the G4 residue and thus the medium to weak NOEs from OH8 to C6H1′ C6H2″ and C6H4′ turned out to be NOEs to the complementary strand.

Chirality of asymmetric carbons of UCH9

The chirality of the asymmetric carbons of UCH9 sidechains was not elucidated in the previous determination of the chemical structure (21). For the hydrophobic sidechain the chirality of C6′ was not determined. As mentioned above, the position of the hydrophobic sidechain relative to DNA is restricted by several strong to medium NOEs. In this position if the chirality of C6′ is *S*, NOEs between H6′ of UCH9 and G4NH and G4NH$_2$ are expected, while none are expected if C6′ is *R*. The experimental observation of these NOEs indicates that the chirality of C6′ is *S*. The chemical structure of the hydrophilic sidechain of UCH9 is the same as those of CHM and MIT and therefore the same stereo configuration as those of CHM and MIT was assumed for the hydrophilic sidechain in the following structure calculation.

Calculation of the complex structure

On the basis of the distance and dihedral angle restraints derived from NOEs and coupling constants, the structure of the UCH9–d(TTGGCCAA)$_2$ complex was calculated by use of X-PLOR. In total 20 structures were calculated, the canonical A-form being used as the starting DNA structure in 10 cases and the canonical B-form in the other 10 cases. Then 12 of the 20 structures were accepted on the criteria of no distance restraint violation of >0.5 Å and no dihedral angle restraint violation of >5°. For the accepted structures root mean square (r.m.s.) deviations from ideal covalent geometry were 0.014 ± 0.002 Å for bond lengths, 1.82 ±

0.20° for bond angles and 0.85 ± 0.16° for impropers. r.m.s. deviations for input distance and dihedral angle restraints were 0.076 ± 0.004 Å and 2.43 ± 0.54° respectively. Figure 6A shows a stereo view of superpositioning of the 12 accepted structures, demonstrating satisfactory convergence. The atomic r.m.s. deviations for heavy atoms between each accepted structure and an average of the 12 accepted structures were 0.77 ± 0.21 Å, the convergence being confirmed quantitatively. The lowest energy structure among the accepted ones is shown in Figure 6B. When only the DNA molecule is considered the atomic r.m.s. deviations were 0.43 ± 0.10 Å for the accepted structures. The atomic r.m.s. deviations between the initial A- and B-form structures was 4.75 . The atomic r.m.s. deviations for the DNA molecule between each accepted structure and the initial A-form structure, the initial B-form structure, the energy-minimized A-form structure and the energy-minimized B-form structure were 4.69 ± 0.21, 1.97 ± 0.05, 4.67 ± 0.21 and 1.82 ± 0.05 Å respectively.

Table 2. NOEs between two segments of UCH9 in the complex[a]

	ChmH5[b]	ChmH10	ChmH4a	H7′	Me6′	H8′	OMe1′
AH1	s		m			m	
AH2e					w		
AH3	w						
AH5	w	w					
AH6	m	m					
BH3	w	w					
BH5			m				
BH6							m
CH1	m	w					
CH3	w	w					
CH4	m	w					
CH5	s	s					
CH6	w	w					
DH1	w			w		w	
DH2e				w		w	
DH3						w	
EH1				w		m	
EH2a						w	
EH2e						w	
EH3					w	w	
EH5						w	

	AH2a	AH4	AH6	BH3	DH1	EH1
CH2a				s		
CH2e				s	m	
CH3				s	m	
CH4			w		m	
DH1	w	w	m			
DH2e						m
DH3						m
DH5		w	m			
EH6	w					

[a]Strong, medium and weak NOEs are denoted by s, m and w.
[b]Chm indicates chromophore.

Table 3. Intermolecular NOEs between UCH9 and d(TTGGCCAA)$_2$ in the complex[a]

UCH9	d(TTGGCCAA)$_2$							
		H2	H1′	H2″	H4′	H5′/H5″	NH	NH_2
ChmOH8	G4						w	s
ChmOH8	C5		m		m			
ChmOH8	C6		m	w	w			
ChmH3	C6					m		
ChmH5	C5				w	m		
ChmH10	C5				m			
H6′	G3							m
H6′	G4						m	m
H7′	G3							m
Me6′	G4		s		s		m	m
Me6′	C5		m			m		
H8′	G3							m
H8′	C6		w	w				
H8′	A7	w	m		w	w		
AH1	C5					m		
AH2e	G4				m			
BH1	C6				w			
BH2a	C6				w			
BH2e	C6				w			
BH3	C6				w			
BH4	C6			w				
DH2a	A7				w			
DH2e	A7				w			
DH4	A7		m					
DH4	A8				w			
DH6	A8				w			
EH2a	A8				w			
EH2e	A7	w						
EH2e	A8		w		w			
EH3	A7	w						

[a]Strong, medium and weak NOEs are denoted by s, m and w respectively.

DISCUSSION

Overall structure of the UCH9–d(TTGGCCAA)$_2$ complex

As can be clearly seen in Figure 6B, a UCH9 dimer binds along the minor groove of d(TTGGCCAA)$_2$. This result of the structure calculation is consistent with the disappearance of the photo-CIDNP signal for G4H8 on complex formation.

The chromophore of UCH9 is located at around the central segment of DNA and O8 of the chromophore and an exposed amino proton, NH_{2e}, of G4 are close enough to form a hydrogen bond. In the following discussion, this interaction between G4NH_{2e} and ChmO8 is taken as the basis when referring to interactions of one UCH9 monomer with two DNA strands discriminatively. Interaction of one UCH9 monomer with the DNA residue which belongs to the strand to which G4 interacting with that UCH9 monomer belongs is defined as interaction with ‘the same strand’. Interaction of that UCH9 monomer with the DNA residue belonging to another DNA strand is defined as interaction with ‘the complementary strand’. Rings B–E extend in the 3′-direction of the same strand along the minor groove of DNA, being close to C6 and A7 of the same strand. The A ring

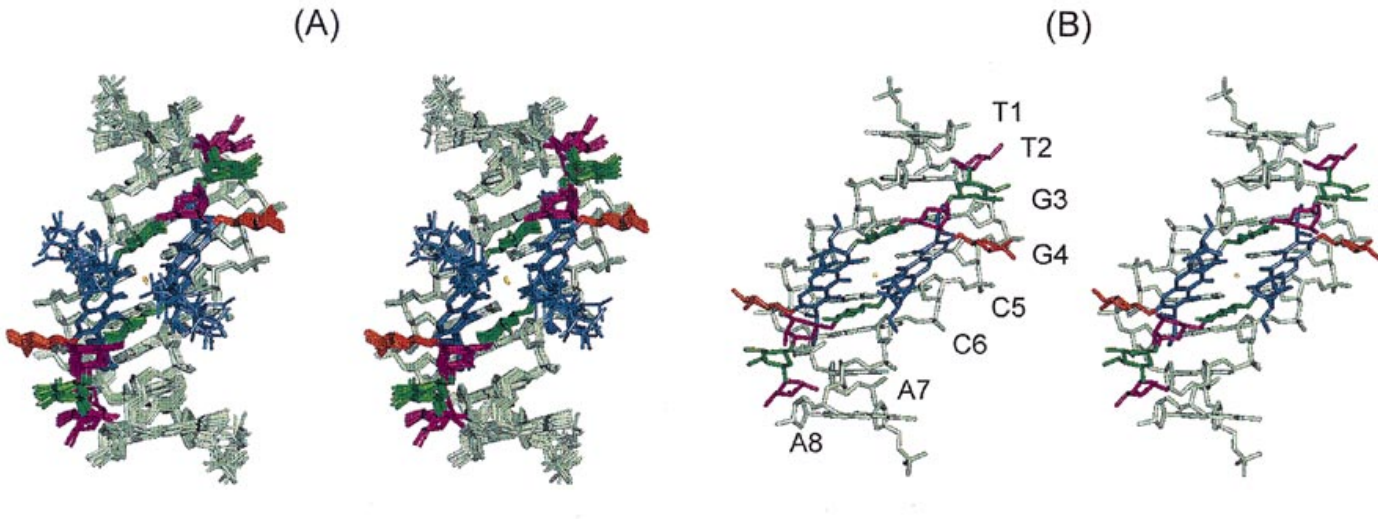

Figure 6. (**A**) A stereoview of superpositioning of the 12 accepted structures of the UCH9–d(TTGGCCAA)$_2$ complex. (**B**) The structure with the lowest energy. DNA, light green; chromophore, blue; A ring, orange; B and D rings, green; C and E rings, purple.

is located between G4 and C5 of the same strand. The hydrophilic sidechain also extends in the 3′-direction, being close to C6 of the same strand. The hydrophobic sidechain extends in the 5′-direction, being close to G3 and G4 of the same strand and additionally to C6 and A7 of the complementary strand. C5H4′ is stacked on the aromatic ring of the chromophore of UCH9, this being consistent with its remarkable upfield shift by 2.34 p.p.m. on complex formation.

Accommodation of a drug dimer in the minor groove of DNA was observed for the CHM–DNA and MIT–DNA complexes as well (13–19). Positioning of the chromophore at around the central segment of DNA and the direction of extension of ring A and rings B–E (the A and B rings and rings C–E in the cases of CHM/MIT) and the hydrophilic sidechain along the minor groove are also similar to those observed in the CHM–DNA and MIT–DNA complexes.

Structural change of DNA on binding of UCH9

On binding of UCH9 the sugar conformations of C5 and C6 changed from C2′-*endo*, which is the sugar conformation of the canonical B-form, to C4′-*exo*, which is close to the C3′-*endo* of the canonical A-form. The minor groove of the A-form is wider than that of the B-form (38). Thus it is supposed that a B to A conformational change of the C5–C6 segment was induced to accommodate the bulky UCH9 dimer in the minor groove.

In the cases of CHM–DNA complexes CHM–d(AAGGCCTT)$_2$ (15), CHM–d(TTGGCCAA)$_2$ (13) and CHM–d(GGGGCCCC)$_2$ (24) the central four residues from G3 to C6 were all C3′-*endo*. It is suggested that this is because a greater structural change in the A-form and a resulting wider minor groove are required to accommodate a CHM dimer in comparison with a UCH9 dimer. In order to examine this notion the width of the minor groove was compared. The width of the minor groove, defined as the shortest phosphorous–phosphorous distance across the minor groove, is 11.5 Å for the canonical B-form and 16.2 Å for the canonical A-form. The only CHM–DNA complex for which atomic coordinates are available is CHM–d(AAGGCCTT)$_2$. The width is 15.1–15.4 Å for the central region of CHM–d(AAGGCCTT)$_2$, while it is 13.3–14.4 Å for the central region of UCH9–DNA. The minor groove is wider than that of the B-form in both complexes, to accommodate a drug dimer, but more pronounced widening is observed for the CHM–DNA complex, as expected.

In the case of MIT–d(ACCCGGGT)$_2$ A-form sugar puckering was found for C3, C4, G6 and G7 (18), in the case of MIT–d(TGGCCA)$_2$ C4 was C3′-*endo* (16) and in the case of MIT–d(TCGCGA)$_2$ T1, C2 and C4 showed A-form sugar puckering (16). It seems that a MIT dimer was accommodated with less structural change in the DNA in comparison with accommodation of a CHM dimer. In fact, the width of the minor groove of MIT–d(TCGCGA)$_2$, for which atomic coordinates are available, is less in comparison with that of CHM–d(AAGGCCTT)$_2$.

In UCH9–d(TTGGCCAA)$_2$ the sugar conformations of G3 and G4 remained in the B-form. Thus for the central G3–C6/G3–C6 region, the two complementary segments of a duplex, the G3–G4 and C5–C6 segments are structurally heterogeneous, the former taking on the B-form and the latter the A-form. In the case of CHM–DNA complexes both segments took on the A-form in the central G3–C6/G3–C6 region without such heterogeneity. Partial heterogeneity was observed for the MIT–DNA complexes (16,18).

UCH9 dimer structure in the complex and its comparison with the CHM dimer structure

A greater structural change in DNA on complex formation was observed for CHM than for UCH9. In order to understand the origin of the difference in structural change, the dimer structures of the two drugs in complex were compared.

Position of the C ring. The positions of the B and C rings relative to the chromophore in the UCH9 dimer were determined from many NOEs between the B and C rings and the chromophore (Table 2). On the basis of the obtained UCH9 dimer structure (Fig. 7C), the high field shifts of H3 of the B ring and H1 of the

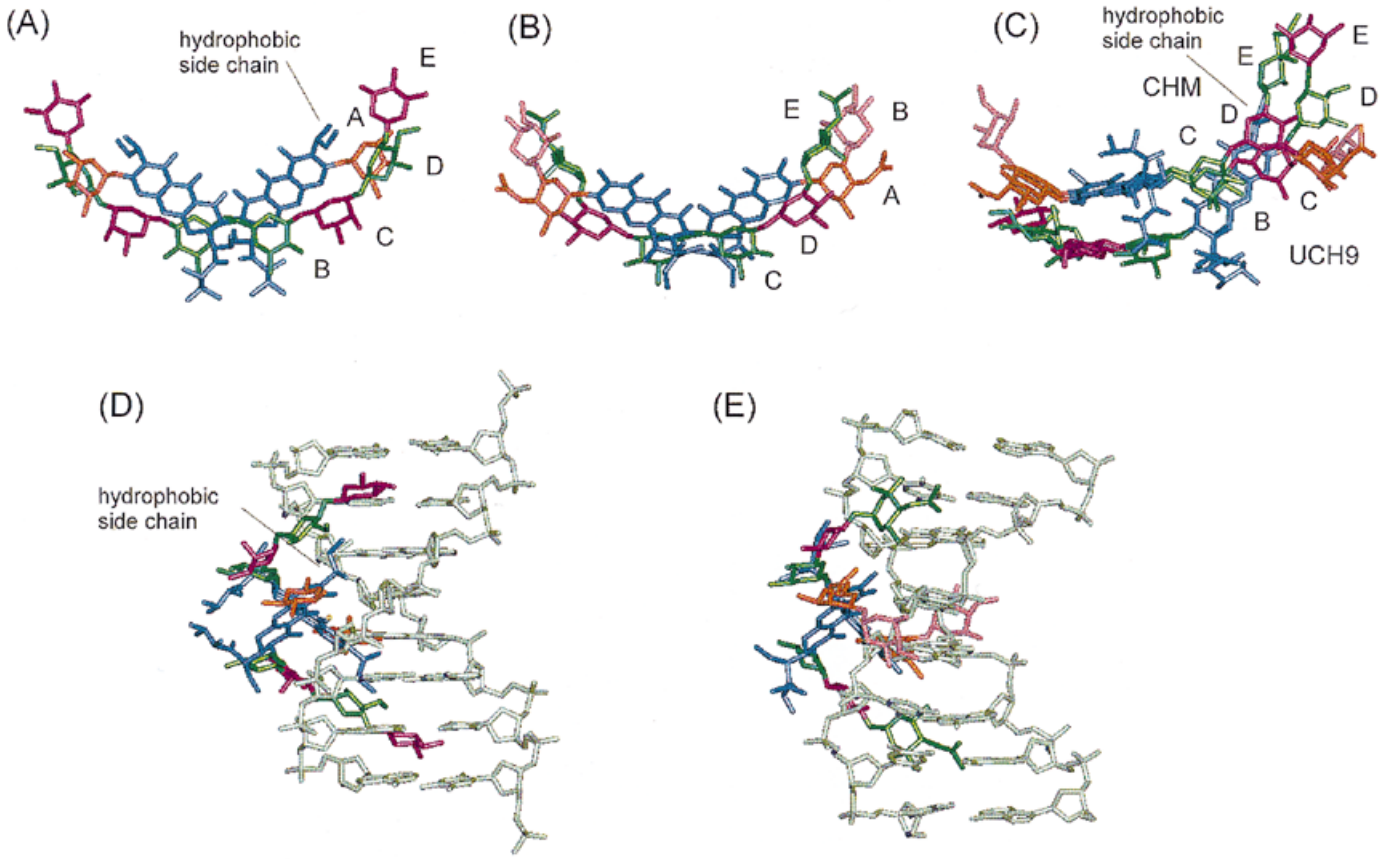

Figure 7. (**A**) UCH9 dimer structure in the complex, viewed roughly from the top of the DNA helix. See also Figure 6D for reference. Chromophore, blue; A ring, orange; B and D rings, green; C and E rings, purple. (**B**) CHM dimer structure in the complex (15). Chromophore, blue; A ring, orange; B ring, pink; C and E rings, green; D ring, purple. (**C**) Comparison of the UCH9 and CHM dimer structures. The chromophores of UCH9 and CHM are superimposed. (**D**) Structure of UCH9–d(TTGGCCAA)$_2$. DNA, light green. (**E**) Structure of CHM–d(AAGGCCTT)$_2$.

C ring (Table 1) are rationalized as the consequence of a ring current effect of the aromatic ring of the chromophore.

O8 of the chromophore of UCH9 is thought to form a hydrogen bond with NH_{2e} of G4 and the same hydrogen bond was suggested for the CHM–DNA complex (15). Therefore, the position of the chromophore can be regarded as an internal reference for estimating the distance between each segment of the drug and DNA. Thus it should be noticed in Figure 7A and B that the C ring of UCH9 is located further from the DNA than the corresponding D ring of CHM. This difference is caused by replacement of a methyl group (Me7) of CHM by the much more bulky hydrophobic sidechain of UCH9. In the case of UCH9, due to steric hindrance between the bulky hydrophobic sidechain and the C ring (Fig. 7C), the C ring is located outward, being apart from the DNA, in comparison with the corresponding D ring of CHM.

Position of the D ring. The D ring of UCH9 is also located further from the DNA than the corresponding E ring of CHM. This is partly due to the difference in absolute configuration of the ring. All rings of UCH9, including the D ring, take on the D configuration, while the corresponding E ring of CHM takes on the L configuration, the others of CHM taking on the D configuration. Thus the E ring of CHM is located closer to the DNA, while the corresponding D ring of UCH9 is located apart from the DNA (Fig. 7A and B). Steric hindrance with the hydrophobic sidechain also causes the D ring of UCH9 to be located apart from the DNA (Fig. 7C). Instead, the D ring of UCH9 is located close to the A ring of another UCH9 monomer (Fig. 7A), as supported by the many NOEs between the D ring and the A ring (Table 2). The following E ring of UCH9 is also located apart from the DNA.

Hydrophobic interaction. It is implied that the hydrophobic interaction involving the hydrophobic sidechain and hydrophobic portions of the A, D and E rings contributes to stabilization of the UCH9 dimer (Fig. 7A and C). The hydrophobic sidechain and the ring corresponding to the E ring of UCH9 are lacking in the chemical structure of CHM. Additionally, the E ring of CHM (which corresponds to the D ring of UCH9) is located close to the DNA, being apart from the A ring. Thus the hydrophobic interaction must be weak in the CHM dimer, if it exists at all (Fig. 7C). Stabilization by the hydrophobic interaction may account for the significantly high binding constant of Mg^{2+} to UCH9, because once the UCH9 dimer is formed with coordination of Mg^{2+} the dimer would be very stable and Mg^{2+} cannot be released from the dimer.

Differences in interaction with DNA and induced structural changes to DNA among the three drugs

In the case of the CHM–DNA complex (15), because of the inward positioning of the D and E rings, the E ring is close to G3 and G4 of the complementary strand (Fig. 7B and E). In the case of the UCH9–DNA complex, in contrast, the D ring (which corresponds to the E ring of CHM) and the following E ring are distant from G3 and G4 of the complementary strand (Fig. 7A and D), because of the outward positioning of the corresponding C and D rings. The absence of a NOE between the D/E rings and G3/G4 (Table 3) supports a mutually distant location. The NOEs concerning the D/E rings are only those to A7/A8 of the same strand (Table 3).

Instead of the NOE from the D/E rings, G3/G4 receive many NOEs from the hydrophobic sidechain (Table 3). This is reasonable, because the hydrophobic sidechain is located inward, being close to G3/G4 of the DNA, in comparison with the D/E rings (Fig. 7A and D), i.e. interaction of G3/G4 with the E ring in the CHM–DNA complex is replaced by that with the hydrophobic sidechain, which is located deeper in the minor groove than the D/E rings, in the UCH9–DNA complex. Generally a monosaccharide is more bulky than the hydrophobic sidechain of UCH9. In particular, the E ring of CHM is rather bulky, due to the sidechain attached to it. Thus it is suggested that inducement of a larger structural change in DNA was necessary for the CHM–DNA complex to accommodate the more bulky E ring, while inducement of a moderate structural change was enough for the UCH9–DNA complex to accommodate the less bulky hydrophobic side chain.

Concerning the MIT–DNA complex, the positions of the C and D rings of MIT are supposed to be similar to those of CHM, as supported by the fact that the NOEs between the C/D rings and the chromophore observed for MIT are very similar to those observed for CHM (18). Although the absolute configuration of the E ring of MIT is the D configuration, like that of the corresponding D ring of UCH9, the E ring of MIT still manages to be in contact with the DNA (16,18). This may be because the absence of the hydrophobic sidechain in MIT allows its D and E rings to be located inward in comparison with the corresponding C and D rings of UCH9. In contrast to the E ring of CHM, the E ring of MIT gave NOEs to the A ring (18). Therefore, the MIT E ring may be located outward in comparison with the CHM E ring. Thus the position of the MIT E ring in the minor groove seems to be intermediate between those of the CHM E ring and the corresponding UCH9 D ring, which is consistent with less structural change in DNA by MIT in comparison with that by CHM.

Correlation between the biochemical and structural results

A wider minor groove is required to accommodate the more bulky CHM dimer than the UCH9 dimer. To achieve the wider minor groove four residues change their sugar conformations from the B-form to the A-form in CHM–DNA complexes, while only two residues change their sugar conformations in the UCH9–DNA complex. The structural change from the B-form to the A-form is accompanied by DNA unwinding (38). Thus the structural change detected spectroscopically must correlate with the DNA unwinding detected biochemically on agarose gel electrophoresis. In fact, greater DNA unwinding was observed biochemically on binding of CHM than on binding of UCH9. An intermediate structural change on binding of MIT was supposed spectroscopically, being consistent with the biochemical result that DNA unwinding by MIT was intermediate between that by CHM and UCH9.

A structural parameter, twist, is related directly to DNA unwinding (38). However, the twist of a short deoxyoligonucleotide such as d(TTGGCCAA)$_2$ is affected by fraying at both ends. Additionally, twist is one of the most difficult parameters to determine accurately by NMR. Therefore twist values obtained from NMR structures must be treated with caution. Twist of the canonical B-form is 36° and if 10.5 bp per turn is assumed in solution it is 34.2°. Average twist for CHM–(AAGGCCTT)$_2$ was 29.8° and that for UCH9–d(TTGGCCAA)$_2$ was 31.8°. It was 30.6° and 31.2° respectively when the average was taken for the central six residues. Twist values <36° (or 34.2°) are consistent with the DNA unwinding detected biochemically. The smaller twist for CHM–DNA in comparison with that for UCH9–DNA may also be consistent with the greater DNA unwinding observed on addition of CHM, although the inaccuracy in twist determined by NMR precludes a decisive conclusion.

Possible relation of the current results with antitumor activity

It was reported that MIT suppresses binding of transcription factor Sp1 to a c-*myc* promoter region (12). It was suggested that MIT inhibits transcription of the c-*myc* protooncogene by suppressing binding of important regulatory factors such as Sp1 (12). Most regulatory factors bind to the major groove. The major groove of the A-form is narrower than that of the B-form (38). Therefore, it is possible that MIT causes a structural change in the promoter DNA from the B-form to the A-like form and thus suppresses binding of the regulatory factors, because the major groove of the induced structure is not wide enough to accommodate the regulatory factors. The same mechanism for antitumor activity may be postulated for CHM and UCH9, because both drugs cause a structural change in DNA to the A-like structure. It should be noted that CHM, which exhibits a more pronounced structural change in the A-like structure than UCH9, shows higher antitumor activity than UCH9 (21). A correlation between the extent of the induced structural change in the A-like structure and antitumor activity may thus exist.

The structure of DNA could be changed to a greater degree by unwinding. There is another possibility, that antitumor activity is correlated with a large scale structural change in DNA.

ACKNOWLEDGEMENTS

M.K. was supported by Grants-in-Aid (nos 09235209, 09680648 and 06276103) from the Ministry of Education, Science, Sports and Culture of Japan and a grant from the Kato Memorial Bioscience Foundation. We wish to thank Professor R.E.Dickerson for providing the NEWHEL93 program, Professor H.Shindo and Dr M.Shimizu for helpful discussions and Mr S.Kakita, Dr Y.Oda, Mr N.Hiraoka and Dr A.Asai for their technical assistance.

See supplementary material available in NAR Online.

REFERENCES

1 Miyamoto,M., Morita,K., Kawamatsu,Y., Noguchi,S., Marumoto,R., Tanaka,K., Tatsuck,S., Nakanishi,K., Nakadaira,Y. and Bhacca,N.S. (1964) *Tetrahedron Lett.*, 2355–2377.
2 Theim,J. and Meyer,B. (1981) *Tetrahedron*, **37**, 551–558.
3 Silva,D.J. and Kahne,D.E. (1993) *J. Am. Chem. Soc.*, **115**, 7962–7970.
4 Silva,D.J., Goodnow,R.,Jr and Kahne,D.E. (1993) *Biochemistry*, **32**, 463–471.

5 Aich,P. and Dasgupta,D. (1990) *Biochem. Biophys. Res. Commun.*, **173**, 689–696.
6 Aich,P., Sen,R. and Dasgupta,D. (1992) *Biochemistry*, **31**, 2988–2997.
7 Aich,P. and Dasgupta,D. (1995) *Biochemistry*, **34**, 1376–1385.
8 Majee,S., Sen,R., Guha,S., Bhattacharyya,D. and Dasgupta,D. (1997) *Biochemistry*, **36**, 2291–2299.
9 Fox,K. and Howard,M.R. (1985) *Nucleic Acids Res.*, **13**, 8695–8714.
10 Ward,D.C., Reich,E. and Goldberg,I.M. (1965) *Science*, **149**, 1259–1263.
11 Yarbo,J.W., Kennedy,B.J. and Barnum,C.P. (1968) *Cancer Res.*, **26**, 36–39.
12 Synder,R.C., Ray,R., Scott,B. and Miller,D.M. (1991) *Biochemistry*, **30**, 4290–4297.
13 Gao,X. and Patel,D.J. (1989) *Biochemistry*, **28**, 751–762.
14 Gao,X. and Patel,D.J. (1990) *Biochemistry*, **29**, 10940–10956.
15 Gao,X., Mirau,P. and Patel,D.J. (1992) *J. Mol. Biol.*, **223**, 259–279.
16 Sastry,M. and Patel,D.J. (1993) *Biochemistry*, **32**, 6588–6604.
17 Sastry,M., Fiala,R. and Patel,D.J. (1995) *J. Mol. Biol.*, **251**, 674–689.
18 Keniry,M.A., Banvile,D.L., Simmonds,O.M. and Shafer,R. (1993) *J. Mol. Biol.*, **231**, 753–767.
19 Banville,D.L., Keniry,M.A. and Shafer,R.H. (1990) *Biochemistry*, **29**, 9294–9304.
20 Ogawa,H. Yamashita,Y., Katahira,R., Chiba,S., Iwasaki,T., Ashizawa,T. and Nakano,H. (1998) *J. Antibiotics*, submitted for publication.
21 Katahira,R., Uosaki,Y., Ogawa,H., Yamashita,Y., Nakano,H. and Yoshida,M. (1998) *J. Antibiotics*, submitted for publication.
22 Huang,H.W., Li,D. and Cowan,J.A. (1995) *Biochimie*, **77**, 729–38.
23 Katahira,M., Sakaguchi-Katahira,R., Hayashi,F., Uesugi,S. and Kyogoku,Y. (1991) *J. Am. Chem. Soc.*, **113**, 8647–8651.
24 Sakaguchi,R., Katahira,M., Fujii,S. and Kyogoku,Y. (1991) *J. Biochem.*, **109**, 317–327.
25 Katahira,M., Sugeta,M., Kyogoku,Y. and Fujii,S. (1990) *Biochemistry*, **29**, 7214–7222.
26 Fresht,A. (1985) *Enzyme Structure and Mechanism.* W.H.Freeman and Co., New York, NY.
27 Hirose,S. and Suzuki,Y. (1988) *Proc. Natl. Acad. Sci. USA*, **85**, 718–722.
28 Hemmerich,P. (1964) *Helv. Chim. Acta*, **47**, 464–475.
29 Jeener,J., Meier,N.H., Bachmann,P. and Ernst,R.R. (1979) *J. Chem. Phys.*, **71**, 4546.
30 Lippens,G., Dhalluin,C. and Wieruszeski,J.-M. (1995) *J. Biomol. NMR*, **5**, 327–331.
31 Rance,M., Sorensen,O.W., Bodenhausen,G., Wagner,G., Ernst,R.R. and Wüthrich,K. (1983) *Biochem. Biophys. Res. Commun.*, **117**, 479.
32 Greisinger,C., Sorensen,O.W. and Ernst,R.R. (1985) *J. Am. Chem. Soc.*, **107**, 6394.
33 Brünger,A.T. (1990) *X-PLOR Version 3.1 User Manual*. Yale University, New Haven, CT.
34 Arnott,S. and Hukins,D.W. (1972) *Biochem. Biophys. Res. Commun.*, **47**, 1504–1509.
35 Kaptein,R. (1982) *Biological Magnetic Resonance*. Plenum, New York, NY.
36 Wüthrich,K. (1986) *NMR of Proteins and Nucleic Acids.* John Wiley and Sons Inc., New York, NY.
37 Hosur,R.V., Ravikumar,M., Chary,K.V.R., Sheth,A., Govil,G., Zu-kun,T. and Todd Miles,H. (1986) *FEBS Lett.*, **205**, 71–76.
38 Saenger,W. (1984) *Principles of Nucleic Acid Structure.* Springer-Verlag, New York, NY.
39 Rinkel,L.J. and Altona,C. (1987) *J. Biomol. Struct. Dyn.*, **4**, 612–649.